

## The NMR structure of the p62 PB1 domain, a key protein in autophagy and NF- $\kappa$ B signaling pathway

Tomohide Saio · Masashi Yokochi ·  
Fuyuhiko Inagaki

Received: 30 June 2009 / Accepted: 14 August 2009 / Published online: 29 August 2009  
© Springer Science+Business Media B.V. 2009

### Biological context

In eukaryotic cells, proteins are degraded via two main pathways; One is the ubiquitin-proteasome system that degrades short-lived proteins, and the other is autophagy that degrades long-lived proteins and damaged organelles (Noda et al. 2009). The p62, also called ZIP (PKC- $\zeta$ -interacting protein) or sequestosome 1, plays a crucial role in these protein degradation pathways (Sumimoto et al. 2007). In autophagy, polyubiquitinated aggregated proteins and damaged organelles are enclosed by the isolation membrane, eventually enwrapped by the autophagosome. The autophagosome is fused with the vacuole/lysosome and its inner content is delivered and then degraded. The p62, initially identified as a protein that binds to the SH2 domain of the tyrosine kinase Lck, functions as a receptor protein for aberrant proteins. It contains a PB1 domain at its N terminus, followed by a ZZ-type zinc-finger motif, a LC3 interacting region, and a UBA domain at its C-terminus (Geetha and Wooten 2002). The p62 interacts with ubiquitin through the UBA domain, and self-assembles through the PB1 domain to form large protein aggregates (Bjørkøy et al. 2005). The p62 also binds the autophagy adaptor LC3 through the WXXL motif in the LC3 interacting region (Noda et al. 2008). Defects in autophagy cause accumulation of protein aggregates that contain ubiquitin and p62, leading to severe liver damage such as

steatohepatitis and hepatocellular carcinomas, and neurodegenerative diseases such as Parkinson's disease, Alzheimer disease, and Huntington's disease (Zatloukal et al. 2002). A recent study indicated that the oligomerization through the PB1 domain was important not only in the assembly of the targets, but also in the interaction with LC3 (Bjørkøy et al. 2005). In the ubiquitin-proteasome system, p62 acts as a shuttling factor that transports ubiquitinated proteins to the proteasome, by interaction through the PB1 domain with the proteasome subunits, S5a and Rpt1 (Seibenhener et al. 2004; Geetha et al. 2008).

The p62 also works as a key factor in cell signal transduction. In the NF- $\kappa$ B signaling pathway, p62 controls osteoclastogenesis, T-cell differentiation, and tumor progression, via the PB1–PB1 interaction with PKC $\zeta$  (Geetha and Wooten 2002). Further, p62 controls adipogenesis and obesity via the interaction with ERK (Moscat et al. 2006), and apoptosis via ubiquitinated Caspase 8 (Jin et al. 2009).

The p62 PB1 domain plays a variety of physiological roles, both through the PB1–PB1 interaction, and through “non-canonical” PB1 mediated interactions with proteins lacking the PB1 domain, such as S5a, Rpt1, ERK, and LCK. Thus, p62 PB1 can be expected to have characteristic features not common to other PB1 domains whose structures have been solved.

The PB1 domain is classified into three types, type I, type II, and type I/II (Hirano et al. 2004). Type I contains a motif of 28 amino acid residues with highly conserved acidic and hydrophobic residues named the OPCA motif. Type II contains a conserved lysine residue on the side opposite to the OPCA motif. Type I/II contains the OPCA motif and the conserved lysine residue, and thus can self-interact in a front-to-back topology. The p62 PB1 contains both the OPCA motif and the conserved lysine residue and

T. Saio  
Graduate School of Life Science, Hokkaido University, Sapporo  
001-0021, Japan

T. Saio · M. Yokochi · F. Inagaki (✉)  
Graduate School of Pharmaceutical Sciences, Hokkaido  
University, Sapporo 060-0812, Japan  
e-mail: finagaki@pharm.hokudai.ac.jp

is classified into type I/II. Using both binding motifs p62 PB1 forms a homo-oligomer which makes purification and NMR analysis difficult (Noda et al. 2003). Therefore, we introduced mutations into the OPCA motif of p62 PB1, to prevent the self-assembly and determined the solution structure of this ‘monomerized’ p62 PB1 domain.

## Methods and results

### Mutagenesis of the p62 PB1 domain

To avoid aggregation of p62 PB1, we first designed site-directed mutants and validated these in terms of solubility and oligomeric state. Based on the amino acid sequence alignment, p62 PB1 has both an OPCA motif and a conserved lysine residue (Fig. 2d). We introduced site-directed mutagenesis into the highly conserved residues on the OPCA motif and prepared two mutants: a D67A single mutant and a D67A/D69R double mutant. Using a *E. coli* expression system, both the mutants and the wild type p62 PB1 domain were expressed and purified, and their oligomeric state was validated using a Superdex 75 10/300 GL gel filtration column (GE Healthcare Bio-Sciences). The molecular mass was estimated by comparing with the elution profile of standards from the Gel Filtration Low Molecular Weight Calibration Kit (GE Healthcare Bio-Sciences) (Fig. 1a). The elution volume of the wild type and the D67A mutant was 7.24 ml (void volume) and 11.77 ml (25 kDa), respectively, indicating that these constructs exist as oligomers. On the other hand, the D67A/D69R mutant is largely monomeric: the D67A/D69R mutant was eluted at 12.67 ml (18 kDa), which is roughly consistent with the molecular mass calculated by the amino acid sequence (11.3 kDa). To confirm the monomeric state of the D67A/D69R mutant, the sedimentation velocity analytical ultracentrifugation experiment was applied using a Beckman Optima XL-I analytical ultracentrifuge equipped with an An-60 Ti rotor. Successive interference scans were recorded at 30 s intervals at 40,000 rpm (Fig. 1b) and the data was analyzed using SEDFIT v11.71 (Schuck 2000). The p62 PB1 D67A/D69R exhibited a peak at 1.33 s (11.2 kDa), which closely matches the theoretical value (11.3 kDa), indicating that the D67A/D69R mutant is present as a monomer in solution.

It should be noted that when the D67A/D69R double mutant was concentrated up to 1 mM, it showed a well-dispersed  $^1\text{H}$ - $^{15}\text{N}$  HSQC spectrum, indicating that the D67A/D69R mutant is suitable for solution NMR experiments (Fig. 1c), while the wild type and the D67A single mutant could not be concentrated above 70  $\mu\text{M}$  due to aggregation.

### Sample preparation and NMR spectroscopy

The D67A/D69R mutant of rat p62 PB1 (3–100) was subcloned, under a GST tag and HRV3C protease cleavage site, into a pGSPS vector derived from pET-21 plasmid (Novagen). The isotopically  $^{13}\text{C}$ - and  $^{15}\text{N}$ -labeled protein was expressed by the *E. coli* strain BL21 (DE3) grown in M9 minimal medium containing  $^{15}\text{NH}_4\text{Cl}$  (1 g/l) and  $^{13}\text{C}$ -glucose (2 g/l) as the sole nitrogen and carbon sources. The Cells were cultured to  $A_{600}$  of 0.8 at 37°C and protein expression was induced with isopropyl  $\beta$ -D-1-thiogalactopyranoside to a final concentration of 0.5 mM, after which the cells were cultured for 16 h at 25°C. The GST-fused p62 PB1 D67A/D69R was purified using a glutathione-Sepharose 4B column (GE Healthcare Bio-Sciences), and GST was excised from p62 PB1 D67A/D69R with HRV3C protease. The p62 PB1 D67A/D69R was further purified using a Superdex 75 gel filtration column (GE Healthcare Bio-Sciences). Finally, the p62 PB1 D67A/D69R was concentrated to 1 mM and applied to the NMR experiments. All the NMR measurements were carried out at 25°C and the sample was prepared in 50 mM MES buffer (pH 6.5) with 50 mM NaCl and 10 mM DTT.

Two- and three-dimensional NMR experiments were performed on Varian UNITY inova spectrometers operating at 800 and 600 MHz. The spectra were processed using the NMRPipe program (Delaglio et al. 1995) and data analysis was performed with the help of the Olivia program developed in our laboratory (Yokochi et al. <http://fermi.pharm.hokudai.ac.jp/olivia/>). The  $^1\text{H}$ ,  $^{13}\text{C}$ , and  $^{15}\text{N}$  resonance assignments were carried out using the following set of spectra:  $^1\text{H}$ - $^{15}\text{N}$  HSQC,  $^1\text{H}$ - $^{13}\text{C}$  HSQC, HN(CO)CA, HNCA, CBCA(CO)NH, HNCACB, HNCO, HBHA(CO)NH, HN(CA)HA, HC(C)H-TOCSY, (H)CCH-TOCSY, HbCbCgCdHd, and HbCbCgCdCeHe. Figure 1c shows the  $^1\text{H}$ - $^{15}\text{N}$  HSQC spectrum of p62 PB1 D67A/D69R. All of the backbone amide resonances were assigned except for His1, Leu10, Lys13, Arg21, Phe23, Glu68, Ser76, and Lys89 and nearly all the side-chain resonances could be assigned. The  $^1\text{H}$ ,  $^{13}\text{C}$ , and  $^{15}\text{N}$  chemical shifts were referenced to DSS according to IUPAC recommendations. Interproton distance restraints for structural calculations were obtained from  $^{13}\text{C}$ -edited NOESY-HSQC and  $^{15}\text{N}$ -edited NOESY-HSQC spectra with a 100 ms mixing time. The structure was calculated using the CYANA 2.1 software package (Herrmann et al. 2002). As the input for the final calculation of the three-dimensional structure of p62 PB1 D67A/D69R, a total of 2,082 distance restraints and 122 TALOS-based  $\phi/\psi$  torsion angle restraints were used (Table 1). At each stage, 100 structures were calculated using 30,000 steps of simulated annealing, and a final ensemble of 20 structures was selected based on CYANA target function

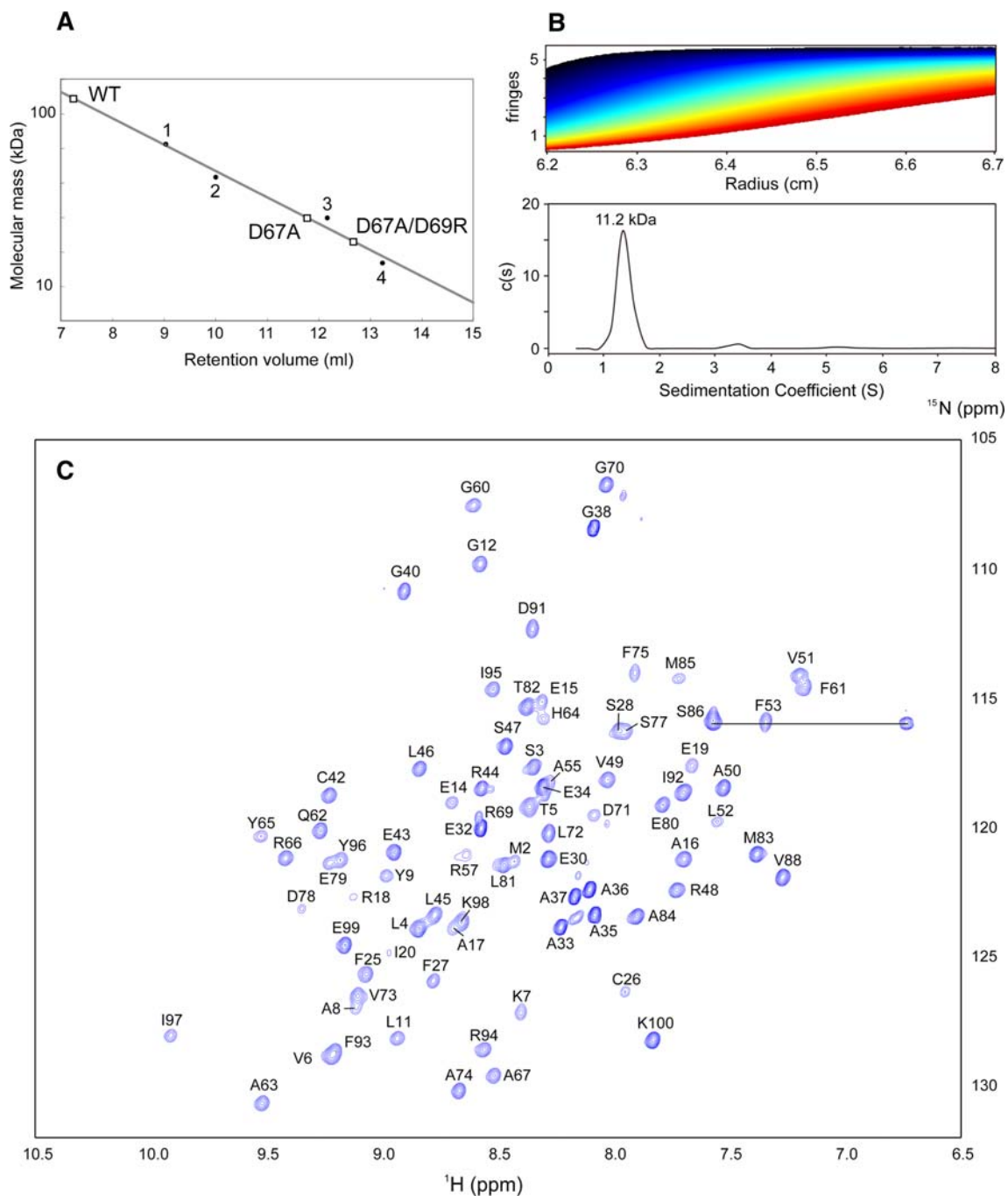


**Fig. 1** **a** The results of analytical size exclusion chromatography of p62 PB1 and its mutants. The p62 PB1 constructs are shown as *squares* and molecular weight standards are shown as *circles*. The calibration curve was constructed from the elution volumes of bovine serum albumin (67 kDa, point 1), ovalbumin (43 kDa, point 2), chymotrypsinogen (25 kDa, point 3), and ribonuclease A (13.7 kDa,

point 4). **b** Sedimentation velocity at the analytical ultracentrifugation of the p62 PB1 D67A/D69R mutant. Successive sedimentation scans were at 30 s intervals (*upper panel*) and the continuous sedimentation coefficient distribution  $c(s)$  (*lower panel*). **c** The  $^1\text{H}$ - $^{15}\text{N}$  HSQC spectrum of p62 PB1 D67A/D69R at 600 MHz and 25°C. The assignments of the backbone amide groups are labeled

values. The atomic coordinates and resonance assignments have been deposited in the Protein Data Bank (PDB code: 2KKC) and BMRB (BMRB code: 16361), respectively.

The structure of p62 PB1 D67A/D69R

An overlay of the 20 structures with the lowest CYANA energy is shown in Fig. 2a. These structures have an

**Table 1** Structural statistics for the 20 structures of ZIP PB1

NOE distance restraints	2,082
Short range (intraresidue and sequential)	1,073
Medium range ( $2 \leq  i - j  \leq 4$ )	324
Long range ( $ i - j  > 4$ )	685
Dihedral angle restraints ( $\phi$ and $\psi$ )	122
Restraint violations	
Distance restraints violated by $>0.3 \text{ \AA}$	0
Torsion angle restraints violated by $>2^\circ$	0
Structural coordinates rmsd <sup>a</sup>	
Backbone atoms ( $\text{\AA}$ )	0.29
All heavy atoms ( $\text{\AA}$ )	0.86
Ramachandran plot (%)	
Most-favored regions	82.2
Additionally allowed regions	17.7
Generously allowed regions	0.1
Disallowed regions	0.0

<sup>a</sup> Analysis applied [for] to the residues except the protease cleavage site (1–3) and flexible loops (12–17, 26–40)

average backbone rmsd of  $0.29 \text{ \AA}$  for the structured region (4–11, 18–25, 41–100) and they present no distance violations of more than  $0.3 \text{ \AA}$  or angle violations larger than  $2^\circ$  (Table 1). The ribbon model of the lowest energy structure of p62 PB1 D67A/D69R is shown in Fig. 2b. The p62 PB1 D67A/D69R contains two  $\alpha$ -helices ( $\alpha 1$ : Pro41-Leu52 and  $\alpha 2$ : Asp78-Tyr87) and a mixed  $\beta$ -sheet composed of five  $\beta$ -strands ( $\beta 1$ : Ser3-Leu11,  $\beta 2$ : Arg18-Cys26,  $\beta 3$ : Phe61-Ala67,  $\beta 4$ : Gly70-Ala74,  $\beta 5$ : Ile92-Glu99). The OPCA motif of p62 (Gly60-Tyr87) has a  $\beta\beta\alpha$  fold and the mutated residues (Ala67 and Arg69) are located on the  $\beta$ -hairpin between  $\beta 3$  and  $\beta 4$ , both pointing to the surface of the protein. The conserved lysine residue (Lys7) is located on the middle of  $\beta 1$  and exposed on the protein surface.

The structure of p62 PB1 D67A/D69R was compared with those of other PB1s deposited in the Protein Data Bank using the Dali search engine (Holm and Sander 1995). The most similar structure was NBR1 (PDB code 2BFK, Z score 11.3), followed by Par6 (PDB code 1WMH, Z score 10.2), p67<sup>phox</sup> (PDB code 2OEY, Z score 10.0), MEK5 (PDB code 2NPT, Z score 10.0), PKC $\iota$  (PDB code 1WMH, Z score 9.9), p40<sup>phox</sup> (z PDB code 1OEY, Z score 9.9), MEKK2 (PDB code 2NPT, Z score 9.7), MEKK3 (PDB code 2O2V, Z score 9.5), Cdc24p (PDB code 1Q1O, Z score 9.2), and Bem1p (PDB code 1IP9, Z score 6.5). The amino acid sequences of these PB1 domains were aligned based on the structural information (Fig. 2d). The two loop regions of p62 PB1 D67A/D69R between  $\beta 1$  and  $\beta 2$ , and between  $\beta 2$  and  $\alpha 1$ , which are less conserved among the PB1s, have low structural convergence as shown in Fig. 2a. We measured the steady-state  $^1\text{H}$ - $^{15}\text{N}$  NOEs at  $25^\circ\text{C}$  with a 3.0 s relaxation delay, using a 600 MHz NMR

spectrometer (Fig. 2c). The  $^1\text{H}$ - $^{15}\text{N}$  heteronuclear NOEs were determined from the ratio of the peak intensities with and without the irradiation of the amide protons ( $I_{\text{on}}/I_{\text{off}}$ ). The NOE values for the two loop regions were lower than those for the structural core, consistent with the structural convergence.

## Discussion and conclusions

Based on the solution structure of p62 PB1 D67A/D69R, the p62 PB1 domain was classified as a type I/II PB1 which can form a homo-oligomer in a front-to-back manner using the OPCA motif and the conserved lysine residue. Although the aPKC PB1 domain is classified as a type I/II, aPKC PB1 does not self-oligomerize and the structure was solved by NMR without mutation, representing the distinct surface properties between p62 PB1 and aPKC PB1 (Hirano et al. 2004). To elucidate the differences in the interaction mode, we compared the electrostatic surface potential of p62 PB1 (Type I/II) to that of PKC $\iota$  PB1 (Type I/II) and Par6 PB1 (Type II) (Fig. 3). The electrostatic surface potential of p62 PB1 was exhibited based on the ‘wild type model’ in which the mutated residues (D67A/D69R) were replaced with the original residues to represent the electrostatic surface potential of native p62 PB1. The acidic residues on the OPCA motif of p62 form two acidic clusters, A1 and A2: Asp67, Glu68, Asp69, and Asp71 form the A1, and Glu79 and Glu 80 form the A2 (Fig. 3a). Among these two clusters, Asp67, Asp69, Asp71, and Glu80 are highly conserved between the type I and type I/II PB1 domains (Fig. 2d). The two acidic clusters, A1 and A2, were common to the type I and type I/II PB1 domains (Fig. 3a, c) (Hirano et al. 2005). The opposite side of p62 PB1 shows a highly basic surface composed of two basic regions, B1 and B2': Lys7, Arg22, and Arg94 form B1, and Arg21 forms B2' (Fig. 3b). The Arg21 and Arg22, the two neighboring basic residues on  $\beta 2$ , direct side chains to opposite directions, forming two distinct basic regions, B2' and B1. The Lys7, that plays a central role in the formation of the B1 basic patch, is highly conserved between type I/II and type II, but conservation of the Arg 21, that forms the B2' patch, is not so high (Fig. 2d). Based on the amino acid sequence alignment, Bem1p and p67<sup>phox</sup> PB1 have no basic residue corresponding to Arg21 of p62, but instead, respectively, have Lys382 and Arg510, located at the C-terminus of  $\alpha 1$ . These residues provide a basic patch, B2, at the structurally similar position to B2' (Wilson et al. 2003; Ogura et al. 2009).

The p62 PB1 has the acidic and basic surfaces highly compartmentalized on either side of the protein, indicating that electrostatic interaction plays an important role in the homo-oligomerization. This electrostatic potential

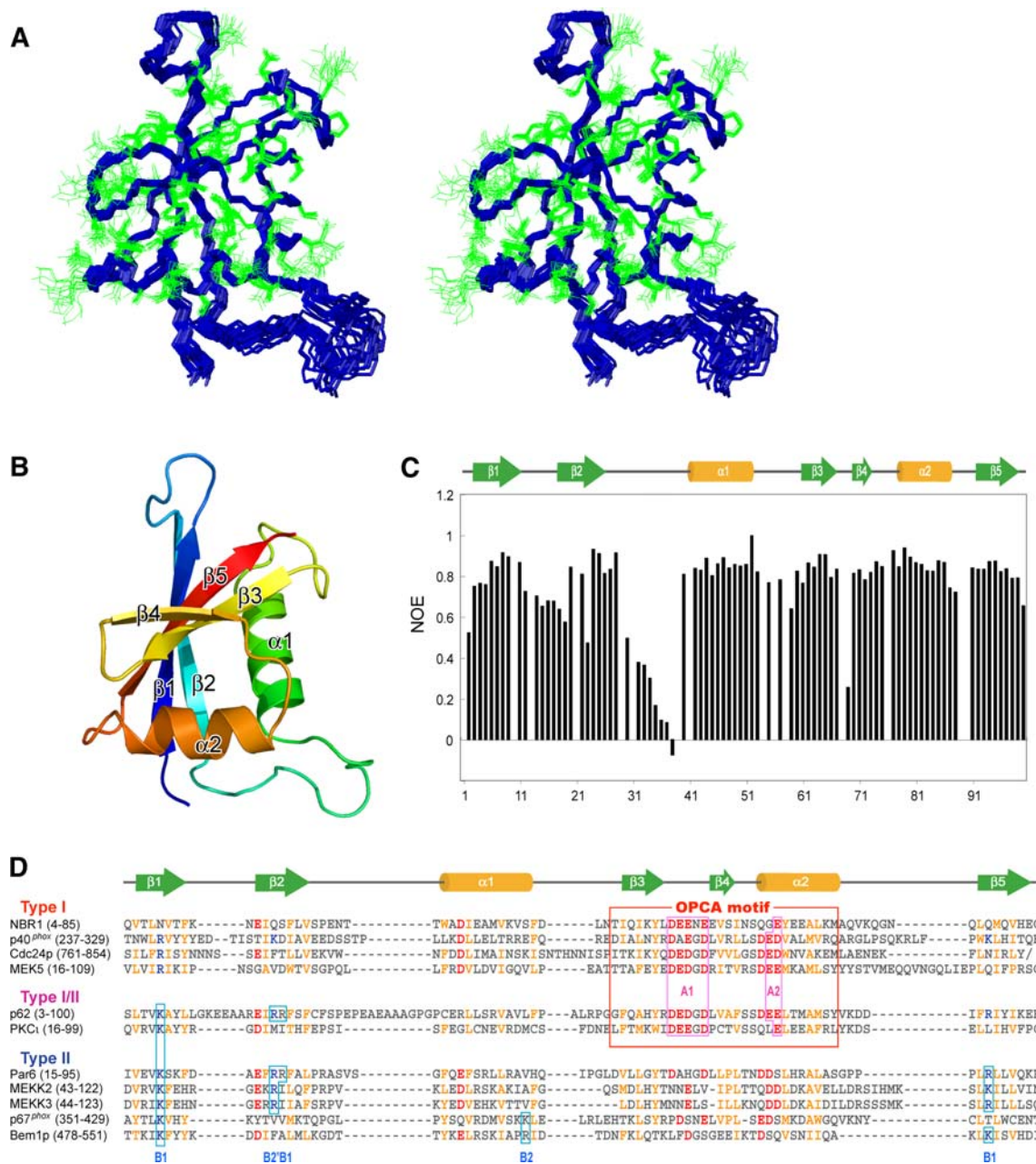


**Fig. 2** **a** Overlay of the ensemble of 20 final energy-minimized CYANA structures in stereo with the heavy atoms superimposed. The side chains in the structured region (4–11, 18–25, 41–100) are shown in *green*. **b** Ribbon representation of the lowest energy structure. The structure is drawn using the MOLMOL (Koradi et al. 1996) and PyMOL programs. **c** The  $^1\text{H}$ – $^{15}\text{N}$  steady-state NOE values of p62

PB1 D67A/D69R, plotted as a function of residue number. **d** Structure-based sequential alignment of the PB1 domain. The conserved hydrophobic residues, acidic residues, and basic residues are highlighted in *orange*, *red*, and *blue*, respectively. The two conserved acidic regions, A1 and A2 (*red*), are boxed, as are the two conserved basic regions, B1 and B2/B2' (*blue*)

compartmentalization is characteristic to p62 PB1 (Fig. 3a, b) and different from the case in PKC $\zeta$  PB1. The OPCA motif of PKC $\zeta$  also forms a highly acidic surface (Fig. 3c), while the basic surface is limited to the smaller region, due to the presence of the acidic residues on the  $\alpha 1$  and the absence of the B2' basic region (Fig. 3d), thus explaining why PKC $\zeta$  PB1 does not self-assemble. To verify the interaction

surface of p62 PB1, we tried to measure the NMR spectra of the wild type and the D67A single mutant of p62 PB1. Although the wild type p62 PB1 was highly oligomeric even at a lower protein concentration (20  $\mu\text{M}$ ), the D67A mutant was less oligomeric and thus we can obtain the subset of  $^1\text{H}$ – $^{15}\text{N}$  HSQC signals of the D67A mutant only at lower protein concentration (30  $\mu\text{M}$ ) with higher ionic

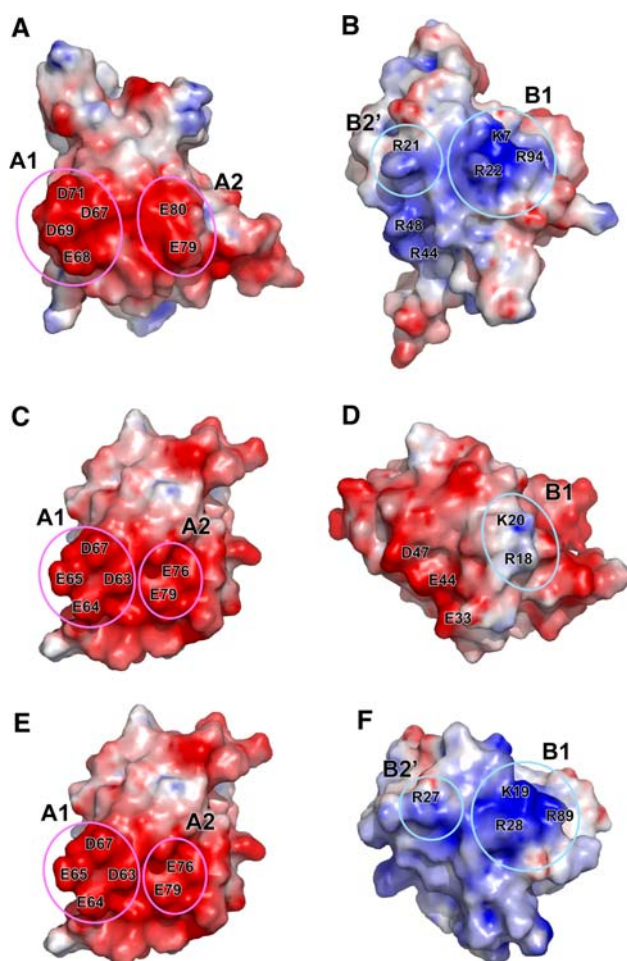


**Fig. 3** Electrostatic surface potential of p62 PB1, PKC $\iota$  PB1, and Par6 PB1. Electrostatic surface potential of the acidic (a) and basic (b) surfaces of the p62 PB1 wild type model, acidic (c, e) and basic (d) surfaces of PKC $\iota$  PB1 (PDB code 1VD2), and (f) basic surface of Par6 PB1 (PDB code 1WMH). The conserved acidic regions, A1 and A2, and the conserved basic regions, B1 and B2', are encircled in magenta and cyan, respectively. Positive and negative charge densities are colored in blue and red. The structure is drawn using the PyMOL program with APBS tools (<http://www.pymol.org>)

strength (250 mM NaCl) (data not shown). The observed signals were derived from the region other than the A1–A2 acidic region and the B1–B2' basic region, indicating the signals from these two regions disappeared presumably due to exchange broadening. These observations are consistent with the expected homo-oligomerization mode of p62 PB1.

The basic surface of p62 (Fig. 3b) resembles that of Par6 PB1 (type II) (Fig. 3f) rather than that of PKC $\iota$  PB1 (type I/II) (Fig. 3d). The Par6 PB1 binds to PKC $\iota$  PB1 and the structure of this complex has been solved (Hirano et al. 2005). In this structure, the A1 and A2 of PKC $\iota$  (Fig. 3e) interact with the B1 and B2' of Par6 (Fig. 3f), respectively. It is to be noted that in the NF- $\kappa$ B signaling pathway, p62 PB1 interacts with aPKC PB1 (Geetha and Wooten 2002; Sumimoto et al. 2007). As the basic surfaces of the Par6 and p62 resemble

each other, it may be speculated that p62 PB1 can bind to aPKC in a similar manner to the PKC $\iota$ -Par6 interaction.

The p62 plays important roles in the ubiquitin-proteasome system, autophagy, and NF- $\kappa$ B signaling pathway, through the PB1–PB1 interaction with its own PB1, Par6 PB1, aPKC PB1, MEK5 PB1, Nbr1 PB1, as well as the non canonical PB1–PB1 interaction with the S5a and Rpt1 subunits of the proteasomes, ERK and LCK. The p62 is also involved in several diseases such as liver damage, neurodegenerative disease, obesity, and cancer. Further structural and biological study will be required for a complete elucidation of the p62-mediated signaling mechanism.

**Acknowledgments** This work was supported by Grant-in-Aid for Scientific Research (Kiban S) and the National Projects on Targeted Proteins Research Programs (TPRP) from Ministry of Education, Culture, Sports, Science and Technology (MEXT), Japan.

## References

- Bjørkøy G, Lamark T, Brech A, Outzen H, Perander M, Overvatn A, Stenmark H, Johansen T (2005) p62/SQSTM1 forms protein aggregates degraded by autophagy and has a protective effect on huntingtin-induced cell death. *J Cell Biol* 171:603–614
- Delaglio F, Grzesiek S, Vuister G, Zhu W, Pfeifer J, Bax A (1995) NMRPipe: a multidimensional spectral processing system based on UNIX pipes. *J Biomol NMR* 6:277–293
- Geetha T, Wooten MW (2002) Structure and functional properties of the ubiquitin binding protein p62. *FEBS Lett* 512:19–24
- Geetha T, Seibenhener ML, Chen L, Madura K, Wooten MW (2008) p62 serves as a shuttling factor for TrkA interaction with the proteasome. *Biochem Biophys Res Commun* 374:33–37
- Herrmann T, Guntert P, Wüthrich K (2002) Protein NMR structure determination with automated NOE assignment using the new software CANDID and the torsion angle dynamics algorithm DYANA. *J Mol Biol* 319:209–227
- Hirano Y, Yoshinaga S, Ogura K, Yokochi M, Noda Y, Sumimoto H, Inagaki F (2004) Solution structure of atypical protein kinase C PB1 domain and its mode of interaction with ZIP/p62 and MEK5. *J Biol Chem* 279:31883–31889
- Hirano Y, Yoshinaga S, Takeya R, Suzuki NN, Horiuchi M, Kohjima M, Sumimoto H, Inagaki F (2005) Structure of a cell polarity regulator, a complex between atypical PKC and Par6 PB1 domains. *J Biol Chem* 280:9653–9661
- Holm L, Sander C (1995) Trends Biochem Sci 20:478–480
- Jin Z, Li Y, Pitti R, Lawrence D, Pham VC, Lill JR, Ashkenazi A (2009) Cullin3-based polyubiquitination and p62-dependent aggregation of caspase-8 mediate extrinsic apoptosis signaling. *Cell*. 2009 May 6
- Koradi R, Billeter M, Wüthrich K (1996) MOLMOL: a program for display and analysis of macromolecular structures. *J Mol Graph* 14:51–55
- Moscat J, Diaz-Meco MT, Wooten MW (2006) Signal integration and diversification through the p62 scaffold protein. *Trends Biochem Sci* 32:95–100
- Noda Y, Kohjima M, Izaki T, Ota K, Yoshinaga S, Inagaki F, Ito T, Sumimoto H (2003) Molecular recognition in dimerization between PB1 domains. *J Biol Chem* 278:43516–43524
- Noda NN, Kumeta H, Nakatogawa H, Satoo K, Adachi W, Ishii J, Fujioka Y, Ohsumi Y, Inagaki F (2008) Structural basis of target recognition by Atg8/LC3 during selective autophagy. *Genes Cells* 13:1211–1218

- Noda NN, Ohsumi Y, Inagaki F (2009) ATG systems from the protein structural point of view. *Chem Rev* 109:1587–1598
- Ogura K, Tandai T, Yoshinaga S, Kobashigawa Y, Kumeta H, Ito T, Sumimoto H, Inagaki F (2009) NMR structure of the heterodimer of Bem1 and Cdc24 PB1 domains from *Saccharomyces cerevisiae*. *J Biochem* (in press)
- Schuck P (2000) Size-distribution analysis of macromolecules by sedimentation velocity ultracentrifugation and lamm equation modeling. *Biophys J* 78:1606–1619
- Seibenhener ML, Babu JR, Geetha T, Wong HC, Krishna NR, Wooten MW (2004) Sequestosome 1/p62 is a polyubiquitin chain binding protein involved in ubiquitin proteasome degradation. *Mol Cell Biol* 24:8055–8068
- Sumimoto H, Kamakura S, Ito T (2007) Structure and function of the PB1 domain, a protein interaction module conserved in animals, fungi, amoebas, and plants. *Sci STKE* 401:re6
- Wilson MI, Gill DJ, Perisic O, Quinn MT, Williams RL (2003) PB1 domain-mediated heterodimerization in NADPH oxidase and signaling complexes of atypical protein kinase C with Par6 and p62. *Mol Cell* 12:39–50
- Zatloukal K, Stumptner C, Fuchsbichler A, Heid H, Schnoelzer M, Kenner L, Kleinert R, Prinz M, Aguzzi A, Denk H (2002) p62 Is a common component of cytoplasmic inclusions in protein aggregation diseases. *Am J Pathol* 160:255–263